IEEE Photonics Journal
An IEEE Photonics Society Publication

Open Access

A Quarter Ellipsoidal Reflector Enhancing Fluorescence Collection Efficiency For Multiphoton Microscopes

Volume 8, Number 5, October 2016

Yingshun Xu
Nannan Liu
Xuehui Bao
Bin Liu
Hui Shen

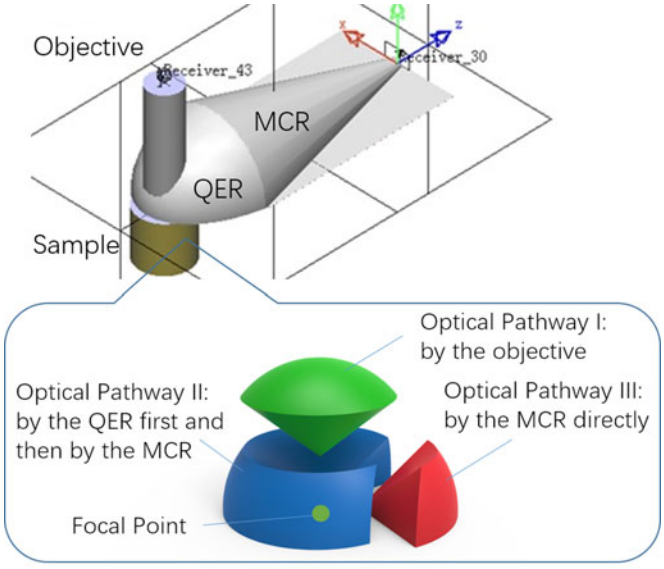

DOI: 10.1109/JPHOT.2016.2615284
1943-0655

A Quarter Ellipsoidal Reflector Enhancing Fluorescence Collection Efficiency For Multiphoton Microscopes

Yingshun Xu, Nannan Liu, Xuehui Bao, Bin Liu, and Hui Shen

School of Biomedical Engineering, Tianjin Medical University, Tianjin 300070, China.

DOI:10.1109/JPHOT.2016.2615284

Manuscript received August 8, 2016; revised September 30, 2016; accepted October 2, 2016. Date of current version October 20, 2016. This work was supported in part by the Scientific Funding of Tianjin Medical University under Grant 2014KYQ17 and in part by Tianjin Research Program of Application Foundation and Advanced Technology Grant 12JCYBJC19500. Corresponding author: Hui Shen (e-mail: huishenlj@hotmail.com).

Abstract: In this paper, we present a fluorescence collection enhancement method for multiphoton microscopy by a quarter ellipsoidal reflector (QER). It is proven to be compatible with commercially available two-photon microscopes without significant customization. The structure and working principle of the QER is demonstrated. A QER was fabricated to collect most backscattered photons not collected by an objective lens of an epifluorescence microscope and then reflected photons into an external detector. Fluorescence collection efficiency improvement of 2.75-fold in numerical simulation is obtained. The method is also validated by imaging turbid phantoms and *ex vivo* biological tissue. Quantum efficiency (QE) corrected experimental results obtained by our method are comparable with those obtained by a nondescanned detection (NDD) scheme of a commercially available multiphoton microscope system. Finally, our method is shown to have potential in neuroscience research for deep tissue imaging.

Index Terms: Non-linear microscopy, biophotonics instrumentation, fluorescence microscopy.

1. Introduction

Multiphoton fluorescence microscopy has been widely used in medical and biological imaging application [1]. Benefiting from better penetration depth of near infrared (NIR) femtosecond laser pulses, multiphoton fluorescence microscopy has performed its capability of imaging deep tissue well [2]–[5]. For multiphoton epifluorescence imaging NIR laser pulses were delivered and confined to the focal region deep into the tissue by an objective with medium numerical aperture (NA) of 0.6-0.8 [6]. As a result fluorescence photons within the focal point were excited isotropically. As an intrinsically turbid media, biological tissue always presented its optical properties as highly scattering and noticeably absorptive. In epifluorescence imaging an objective was used to collect most of reflected ballistic and some backward scattered fluorescence photons, depending on its NA and the objective front aperture (OFA) [7]. However a geometrical collection of only 10% was achieved by a 40 $\times$ 0.8 NA water immersion objective to image turbid media [8].

Several techniques were applied to collect backward scattered fluorescence photons as many as possible. A concept of hybrid objective of a refractive objective surrounded by a reflective conic

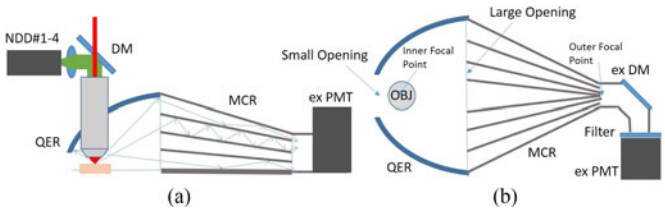

Fig. 1. Schematics of the device. (a) Side view: NDD#1-4: four NDD GaAsP PMTs of Nikon microscope; DM: dichroic mirrors of Nikon microscope; OBJ: objective of Nikon microscope. (b) Top view. (Total setup of Nikon microscope is not shown here).

surface was presented and simulated [8]. A total emission detection (TED) technique using a parabolic reflector performed enhancement of 10-fold in simulation and 8.9-fold in experiment [9]. In this case, fluorescence photons were collimated into a photomultiplier tube (PMT) by a parabola and a refractive lens. Similar results were also reported by using reflective cylindrical surfaces [10]. Improvement of twofold in experimental results and 3 mm imaging depth were obtained by epifluorescence modification of devices mentioned above respectively [11], [12]. Recently a compact design of the TED device was conducted to work with a highly customized upright two-photon microscope [13]. In addition fiber-ring based collection methods were also presented by using five to eight pieces of high NA ($\sim$0.5) optical fibers to circumferentially surround the objective. Improvements were obtained as twofold with high NA objectives and 20-fold with low NA objectives, respectively [14], [15].

As indicated most of reflective collection methods required highly customized microscopes and fiber-ring based devices were difficult to manufacture and assemble. In this paper we present a fluorescence collection enhancement method for multiphoton microscopy by a QER. It was proven to be compatible with commercially available two-photon microscopes without significant customization. Both numerical simulation and experimental results shown in this paper had potential in neuroscience research. The potential could benefit from increased signal-to-noise ratio (SNR) in terms of faster imaging and less photo-damage.

2. Material and Methods

2.1. Optical Setup

Our device was designed and constructed in a small outline to fit the limited operation space beneath the objective turret of a upright Nikon A1R MP microscope system applied in our case. The femtosecond laser source was a Spectral Physics MaiTai Deepsee Titanium Sapphire solid state laser generating NIR laser pulses with the pulse width of 70 fs and the repetition rate of 80 MHz. As illustrated in Fig. 1, the device mainly consisted of three parts, including a QER, a multilayer conical reflector (MCR) and an external PMT module (ex PMT). The small opening, large opening, inner focal point, and outer focal point of QER were also demonstrated in Fig. 1.

In this device, fluorescence emitted isotropically at the focal region might propagate through three pathways to reach both the objective and the ex PMT. Obviously, most reflected ballistic photons and parts of backscattered photons in smaller emitting angles were collected by the objective and detected by the NDD of the Nikon microscope in epifluorescence imaging, which are shown as the green part in Fig. 2. By the second pathway, parts of backscattered photons in larger emitting angles not entered the objective were firstly reflected by the QER, then collected by the MCR, finally head for the outer focal point where the ex PMT located, which is shown as the blue part in Fig. 2. By the third pathway, the remaining backscattered photons were directly emitted through the large opening of the QER and redirected to the ex PMT by the MCR, shown as the blue part in Fig. 2. Additional photons not collected by the objective could transmit through both of the second and the third optical pathway and finally be collected by the ex PMT. That is why our method can increase

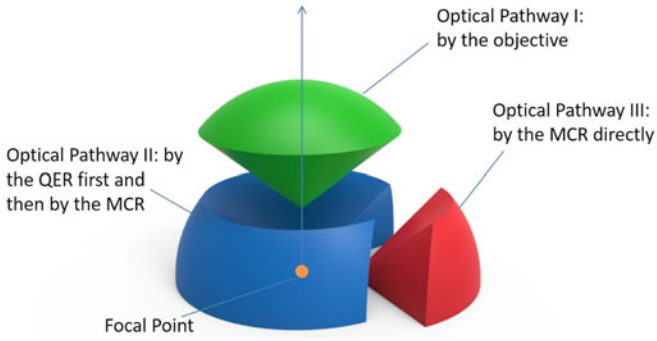

Fig. 2. Optical pathway I (green), II (blue), and III (red) of backward scattered photons. (Three parts are apparently separated for better demonstration.)

the SNR in epifluorescence imaging. The 3-D model of backward propagation of photons shown in Fig. 2 was based on the dimension of our experimental scheme.

The QER was based on a cone-axis ellipsoidal cold reflector (CAECR) originally for xenon light collimation. The CAECR made by quartz had two openings on its two ends, the large opening for releasing collimated light and the small opening for adding water for a 40X water immersion objective (CFI Apo 40XW NIR, Nikon, Japan, NA $=$ 0.8, WD $=$ 3.5 mm). The inner surface of the CAECR was coated with an interference thin film to reflect visible light and transmit NIR light. The average visible light reflection was $\sim$93% while the average NIR transmission was $\sim$85%. The diameter of the CAECR was 97 mm. The distance between its inner focal point and its small opening was 15 mm. The distance between the outer focal point of the CAECR and its small opening was 145 mm. To fabricate a QER, a CAECR was firstly cut into half along the long axis of the ellipsoid. Then a hole was drilled perpendicularly to the optical axis of the CAECR and the center of the hole was precisely aiming at the inner focal point of the CAECR. The hole was used to hold the objective of the microscope.

Why was a QER selected to play an important role for extra photon collection? Because slight modification of a commercial microscope system was the main consideration in our design. Therefore most of backward scattered fluorescence photons should be redirected horizontally to a horizontally located external detector rather than propagated vertically through a highly customized microscope reported by other groups [8]–[13]. Two kinds of reflectors were available, parabolic and ellipsoidal. The focal point of an objective and the inner focal point of a reflector should coincide. As mentioned before, in order to fit in limited space between the turret of the microscope and the translation stage, the height of the reflector should be limited to about 60 mm which was the same as the parfocal length of Nikon objectives. Moreover, a hole must be drilled on the reflector to make the objective approach the imaging target and diameters of most commonly used objectives ranged from 22 mm to 26 mm. However, it was difficult to make such a hole in a sized limited parabolic reflector due to the insufficient distance from its inner focal point to its small end. In our case of a CAECR with 97 mm diameter, the distance from its inner focal point to its small end of 15 mm was enough for making such a hole. Fig. 3 photographically showed fabrication process of a QER as well as its assembly with a Nikon 40X objective. Imaging properties of ellipsoidal reflectors were suitable for this application [16], [17].

The MCR, acting as the light guide for latter two optical pathways aforementioned, was designed and manufactured for following considerations. Only reflective optics was found to be suitable for maximizing scattered photon transmission between a collective optics and a detector, especially in turbid media imaging [8]. The geometry of the MCR should match the semicircular opening of the QER and the rectangular sensitive window (28 mm by 8 mm) of the ex PMT. The MCR was based on a glass substrate (150 mm by 100 mm) coated with an aluminum reflective thin film which has the average reflection of 94%-97% in 400 nm-700 nm wavelength region. Four

Fig. 3 . (a) Cut and (b) drill process to make a QER. (c) Fabricated QER; (d) QER assembled with a 40X objective.

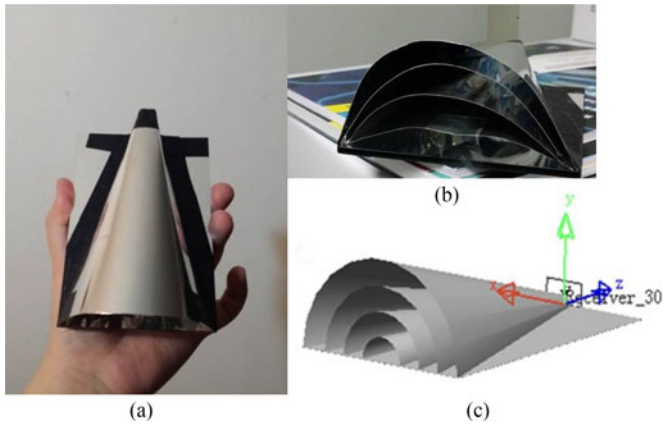

Fig. 4 . (a) Top view, (b) side view, and (c) 3-D model of the MCR.

pieces of double-side mirror polished aluminum foils were molded to form a multi-channel reflector minimizing the reflection of incident light and then fixed on the glass substrate. One opening of the MCR was semicircular while the other opening was nearly rectangular. The actual structure of the MCR is shown in Fig. 4 and its approximate 3-D model was build and simulated. A dichroic mirror (GCC414007, Daheng Optics, Beijing, China, diameter = 25.4 mm) as the external dichroic mirror (ex DM) was a long pass filter with the cut-off wavelength of 660 nm. The ex DM was placed 45° to the incident optical axis.

In the past several wide area head-on PMTs (Hamamatsu R1104, diameter of 25 mm; R7600P-300, 18 mm by 18 mm; H2431, diameter of 60 mm, R2803, diameter of 46 mm) were reported [9]–[13] for enhancing fluorescence detection. However, our design could benefit from the compact outline and low cost of a Hamamatsu CH253 voltage output PMT module. In the PMT module a side-window multi-alkali PMT (CR131, Beijing Hamamatsu, Beijing, China, peak wavelength of 400 nm), a 1250 V high voltage power supply and a low noise amplifier were integrated into a small package of 86 mm by 54.5 mm by 33 mm. There were four NDDs in the Nikon A1R MP microscope and their outputs were transmitted to the microscope controller through four BNC co-axial cables. Only the input of the channel 1 NDD of the microscope controller was replaced by the output of the ex PMT in our study. The channel 2 NDD was also used for conventional epifluorescence imaging. Other two channels NDDs were not involved. The gain of the ex PMT was controlled by a variable voltage ranging from 2 V to 4.5 V by a digitally controlled power supply. Both positive and negative 12 V were required for the ex PMT and supported by the other power supply. All parts were shown in Fig. 5. In addition, a single-band band pass filter (FF01-525/45-25, Semrock, NY, USA) was attached in front of the sensitive window of the ex PMT to block residual NIR. No focusing lens was

Fig. 5. The device, as illustrated in Fig. 1. (a) Overview, (b) side view, and (c) top view. SH:scan head of Nikon microscope; PWR 1&2:power supplies for ex PMT.

applied in front of the ex PMT since that refractive optics were not quite effective for focusing highly scattered photons [8].

2.2. Turbid Media and Tissue Sample Preparation

Turbid samples were prepared by dispersion of fluorescent microspheres (1 μm in diameter, 1% w/v; BaseLine ChromTech Research Centre, China) and polystyrene microspheres (1 μm in diameter, 2.5% w/v; BaseLine ChromTech Research Centre, China) as a scattering agent in a 0.5% agarose gel matrix (Invitrogen, Thermo Fisher Scientific, MA, USA). To obtain samples with excitation scattering lengths of 150 μm at 800 nm [18], which typically found in mammalian brain, 3 μl fluorescent microspheres and 119 μl polystyrene microspheres were added in 1 ml hot agarose gel respectively. As soon as the mixture reached room temperature, it was poured in a custom sample chamber mounted by antifade polyvinylpyrrolidone mounting medium (Beyotime, China) and stored at 4 °C kept in the dark.

For ex vivo tissue imaging, an adult male wild-type C57BL/6 mouse was sacrificed to loading cell populations with calcium-sensitive dye Oregon Green-488 BAPTA-1 (OGB-1; Molecular Probes) AM in brain tissue. The acetoxymethyl (AM) ester of OGB-1 was dissolved in DMSO containing 20% Pluronic F-127 (Invitrogen, Thermo Fisher Scientific, MA, USA) to a final concentration of 10 mM. The stocks were diluted in a solution containing (in mM): 125 NaCl, 2.5 KCl, 10 HEPES, yielding a final dye concentration of 0.5 mM. Based on the improved targeted bulk-loading technique [19], approximately 0.5 μl of the dye-containing solution was injected gradually into the CA1 area of hippocampus (bregma -2.18 mm, lateral -1.20 mm, depth 1.25 mm) over 10 min using a micropipette. Half an hour later, the mice was transcardially perfused with saline and 4% paraformaldehyde (PFA). Mice brain was dissected and post-fixed in 4% PFA for 24 h at 4 °C before cut into suitable coronal section for imaging. All experimental procedures conformed to the Guide for the Care and Use of Laboratory Animals and approved by the Tianjin Medical University Animal Care and Use Committee.

2.3. Numerical Simulation

The fluorescence propagating properties along the objective of the microscope, the QER and the MCR of the device could be analyzed using the numerical ray tracing algorithm by the LightTools software. A 3-D model was created strictly following the schematics shown in Fig. 1. Two light receivers were placed in this model. One located at the back aperture of the objective while the other one was placed at the exit of the MCR. LightTools applied the Henyey-Greenstein distribution

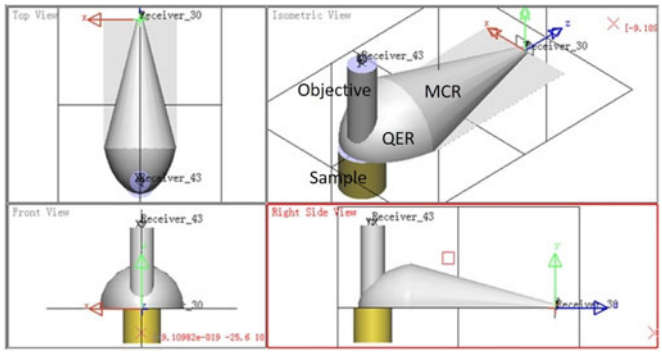

Fig. 6. Four-view graph of the 3-D model for numerical simulation.

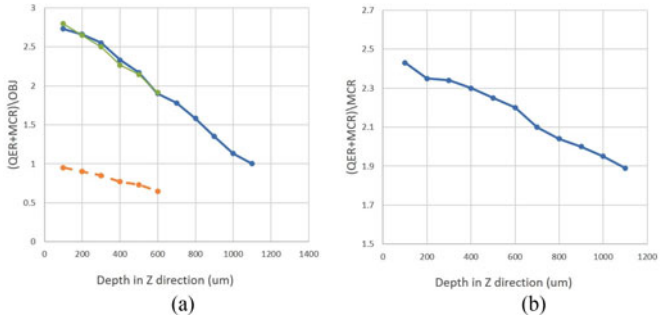

Fig. 7. (a) Ratioof (QER+MCR) to the objective by depth by numerical simulation (blue solid line) and by experiment (orange dot line) and by QE corrected (50/17 $=\sim$ 2.94X) experimental data (green solid line). (b) Ratio of QER+MCR to MCR by depth by numerical simulation.

as the scattering function which is commonly used in biomedical optics. Both absorption and scattering properties of the focal point where fluorescence photons were excited was selected as HumanBrainAdultGreyMatter in the material option of the software. The four-view graph of the 3-D model for numerical simulation including a QER, an MCR, an objective, and a scattering sample was shown in Fig. 6. Two receivers acting as detectors for the objective and the MCR were also included.

3. Numerical and Experimental Results

3.1. Numerical Simulation Results of Fluorescence Collection in Scattering Tissue

In Fig. 7 (a), simulation data,experimental results and quantum efficiency (QE) corrected experimental results of collection efficiency ratio by the QER working together with the MCR into the Nikon 40X water immersion objective were summarized here. According to numerical simulation results maximum ratio of $\sim$2.75-fold was achieved at 100 μm depth in the sample. At 1000 μm depth the gain reduced into $\sim$0.98. In experimental results discussed later the ex PMT showed comparable performance than that of NDDs when the imaging depth was deeper than 700 μm. As discussed in Section 2.1, comparison of the contribution to the total collection between the QER and the MCR was also simulated and presented in Fig. 7 (b). However, it is not possible for us to identify this value experimentally. Fluorescence photons propagating through the second pathway (by the QER and the MCR) were almost two times more than those following the third pathway (by MCR directly). It mainly depended on the geometry of the QER.

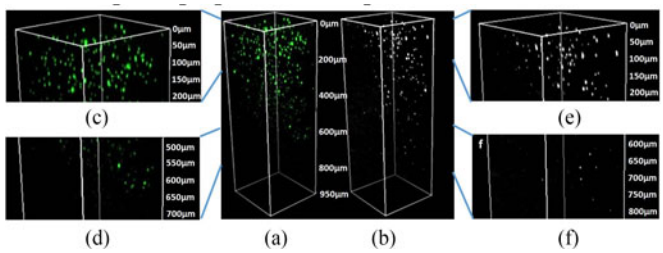

Fig. 8. Three-dimensional volumetric rendered views of two-photon fluorescence images of the turbid sample (a) by NDDs of Nikon microscope and (b) by ex PMT. (c)–(f) Enlarged local details.

3.2. Turbid Media Imaging Results

About 4800 2-D images of a turbid sample were acquired with a 40X water immersion objective both by a NDD and by the ex PMT simultaneously. The imaging depth ranged from 0 μm to 950 μm. The galvano-galvano scanner of the Nikon microscope was used to scan a large number of 2-D images in 512 by 512 pixels. The z scan step was set to be 200 nm. To compensate depth dependent power loss of excitation laser due to scattering, the Z Intensity Correction function of Nikon Element C software was used to generate an interpolated curve of various laser power parameters. 5% at 0 μm, 7% at 550 μm and 9% at 950 μm imaging depth of the NIR laser power of $\sim$2900 mW were appointed by the user to generate the curve and then delivered to the sample. Total image acquisition procedure cost about 2 hours. A 3-D volumetric rendered view was also processed by Nikon Element C software.

Using our detection method it was possible to image fluorescent microspheres in turbid samples at the depth up to $\sim$800 μm shown in Fig. 8(b). Maximum imaging depth of $\sim$600 μm was obtained by the NDD, shown in Fig. 8(a) as a comparison. Images acquired by the NDD revealed more details in top layers while those obtained by the ex PMT showed more in the deeper region. Detailed data were summarized in Fig. 7(a). It should be noted that usually at 500 nm wavelength the QE of GaAsP PMTs was $\sim$50% while that of multi-alkali PMTs was $\sim$17%. If the QE difference of two types of PMTs was taken into consideration, curves presented in Fig. 7(a) almost coincided with each other, but there were still some discrepancies between curves which can be mainly attributed to limited accuracy of the algorithm used in the software, geometrical mismatches of 3-D, models as well as different optical properties of samples.

3.3. Tissue Imaging Results

A wide-field image obtained by a 4X objective on an Olympus IX71 microscope clearly showed positions of the injection channel and the stained cell population in the CA1 of Hippocampus, as shown in Fig. 9 (e). Two-photon images of the *ex vivo* sample were acquired by the same procedure as that used in turbid sample imaging. Since fluorescence by OGB-1 AM was in proportional into the intensity of calcium ion and, in the *ex vivo* sample, the intensity of extracellular calcium ions was always higher than that within neuron somas, somas in the cell population area were shown as darker in Fig. 9(a) and (c) by the NDD and in Fig. 9(b) and (d) by the ex PMT respectively. Stained cell population was showed as surrounding brighter background while a brighter channel represented the injection channel in Fig. 9(c) and (d). Since the fluorescence dye injection method described in Section 2.2 could only stain such a nearly spherical area with the diameter of $\sim$200 μm, only images acquired near the center of the injection target were presented here. In *ex vivo* tissue imaging our method demonstrated its capability of imaging tissue sample and similar performance to that presented in turbid sample imaging.

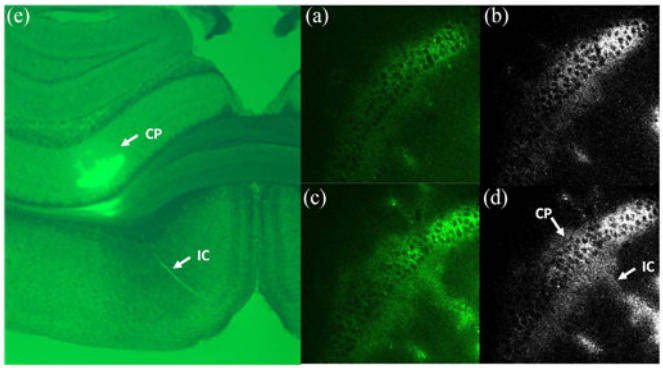

Fig. 9. Images of Hippocampus at 160 μm depth by (a) NDD and (b) ex PMT and at 220 μm depth by (c) NDD and (d) ex PMT. (e) 4X images showed injection channel (IC) and cell population (CP).

4. Discussion

As indicated in Section 2.1, only photons in the optical pathway II and III travel through the MCR. However, due to the reflection of the QER, photons in the optical pathway II definitely have smaller incident angles to the MCR and less reflective times leading to less reflective loss in the MCR. As a comparison, photons in the optical pathway III have larger incident angles to the MCR and more reflective times, and hence suffer from more reflective loss in the MCR. The numerical simulation results of MCR's relative transmittance has been demonstrated in Fig. 7(b).

It could be found that when the imaging depth increases, the collection efficiency improvement by our method is reduced gradually, as shown in Fig. 7(a). When the imaging depth increases, the location of focal point moves deeper into the scattering sample. Since the incident laser power has been increased to compensate its scattering loss, as described in Section 3.2, the excitation laser power at the focal region could be considered as a constant value in this case. The objective collects photons in relative small angles to the incident optical axis and hence shorter travel distance in the sample for less absorption loss. As a comparison, the QER and MCR collects photons in larger angles to the incident optical axis and longer travel distance in the sample for more absorption loss. As a conclusion, the reduction of the improvement could be attributed to the photons collected by QER and MCR suffering from more absorption loss when the imaging depth increases.

The design presented in this manuscript has been proven to enhance the fluorescence collection. Generally faster imaging in optical microscopy always leads to lower SNR. Since more photons could be collected by using our method, SNR definitely could be improved in faster imaging. Based on the same reason, the laser power projected on the sample could be reduced for less photo-damage. That is why the potential could benefit from increased SNR in terms of faster imaging and less photo-damage.

5. Conclusion

The focusing property of a QER made it as the key part for fluorescence collection in our design. We have reported an original method to simply collect more fluorescence photons which could not be collected by an objective in epifluorescence imaging. Maximum improvement of $\sim$2.75-fold was obtained by numerical simulation. The method had also been validated on artificial turbid phantoms. Comparable performance in ex vivo imaging by our device and GaAsP NDDs were demonstrated if the difference of QE of detectors was taken into consideration. This paves the way for a new imaging method of turbid media and showed to have potential for neuroscience research due to significantly increased SNR.

References

[1] W. Denk, J. H. Strickler, and W. W. Webb, "Two-photon laser scanning fluorescence microscopy," *Science*, vol. 248, no. 4951, pp. 73–76, 1990.

[2] W. R. Zipfel, R. M. Williams, and W. W. Webb, "Nonlinear magic: Multiphoton microscopy in the biosciences," *Nature Biotechnol.*, vol. 21, no. 11, pp. 1369–1376, 2003.

[3] E. Beaurepaire, M. Oheim, and J. Mertz, "Ultra-deep two-photon fluorescence excitation in turbid media," *Opt. Commun.*, vol. 188, no. 1–4, pp. 25–29, 2001.

[4] P. Theer, M. T. Hasan, and W. Denk, "Two-photon imaging to a depth of 1000 microm in living brains by use of a Ti:Al2O3 regenerative amplifier," *Opt. Lett.*, vol. 28, no. 12, pp. 1022–1024, 2003.

[5] F. Helmchen and W. Denk, "Deep tissue two-photon microscopy," *Nature Methods*, vol. 2, no. 12, pp. 932–940, 2005.

[6] M. Oheim, E. Beaurepaire, E. Chaigneau, J. Mertz, and S. Champak, "Two-photon microscopy in brain tissue: Parameters influencing the imaging depth," *J.Neurosci. Methods*, vol. 111, no. 1, pp. 29–37, 2001.

[7] E. Beaurepaire and J. Mertz, "Epifluorescence collection in two-photon microscopy," *Appl. Opt.*, vol. 41, no. 25, pp. 5376–5382, 2002.

[8] D. Vučinić, T. M. Bartol, and T. J. Sejnowski, "Hybrid reflecting objectives for functional multiphoton microscopy in turbid media," *Opt. Lett.*, vol. 31, no. 16, pp. 2447–2449, 2006.

[9] C. A. Combs, A. V. Smirnov, J. D. Riley, A. H. Gandjbakhche, J. Knutson, and R. S. Balaban, "Optimization of multiphoton excitation microscopy by total emission detection using a parabolic light reflector," *J. Microscopy*, vol. 228, no. 3, pp. 330–337, 2007.

[10] V. Crosignani, A. S. Dvornikov, and E. Gratton, "Enhancement of imaging depth in turbid media using a wide area detector," *J. Biophoton.*, vol. 4, no. 9, pp. 592–599, 2011.

[11] C. A. Combs *et al.*, "Optimizing multiphoton fluorescence microscopy light collection from living tissue by noncontact total emission detection (epiTED)," *J. Microscopy*, vol. 241, no. 2, pp. 153–161, 2011.

[12] V. Crosignani *et al.*, "Deep tissue fluorescence imaging and in vivo biological applications," *J. Biomed. Opt.*, vol. 17, no. 11, 2012, Art. no. 116023.

[13] C. A. Combs *et al.*, "Compact non-contact total emission detection for in vivo multiphoton excitation microscopy," *J. Microscopy*, vol. 253, no. 2, pp. 83–92, 2014.

[14] C. J. Engelbrecht, W. Göbel, and F. Helmchen, "Enhanced fluorescence signal in nonlinear microscopy through supplementary fiber-optic light collection," *Opt. Exp.*, vol. 17, no. 8, pp. 6421–6435, 2009.

[15] J. D. McMullen, A. C. Kwan, R. M. Williams, and W. R. Zipfel, "Enhancing collection efficiency in large field of view multiphoton microscopy," *J. Microscopy*, vol. 241, no. 2, pp. 119–124, 2011.

[16] K. A. Snail and L. M. Hanssen, "Magnification of conic mirror reflectometers," *Appl. Opt.*, vol. 37, no. 19, pp. 4143–4149, 1998.

[17] M. R. Benson and M. A. Marciniak, "Design considerations regarding ellipsoidal mirror based reflectometers," *Opt. Exp.*, vol. 21, no. 23, pp. 27519–27536, 2013.

[18] J. P. Zinter and M. J. Levene, "Maximizing fluorescence collection efficiency in multiphoton microscopy," *Opt. Exp.*, vol. 19, no. 16, pp. 15348–15362, 2011.

[19] O. Garaschuk, R. I. Milos and A. Konnerth, "Targeted bulk-loading of fluorescent indicators for two-photon brain imaging in vivo," *Nature Protocols*, vol. 1, no. 1, pp. 380–386, 2006. K. E. Petersen, "Silicon torsional scanning mirror," *IBM J. Res. Dev.*, vol. 24, pp. 631–637, Sep. 1980.